PHYSICAL REVIEW E **85**, 015303(R) (2012)

High-speed jetting and spray formation from bubble collapse

Badarinath Karri
NUS Graduate School for Integrative Sciences and Engineering (NGS), Center for Life Sciences, #05-01, 28 Medical Drive, Singapore 117456

Silvestre Roberto Gonzalez Avila
School of Physical and Mathematical Sciences (SPMS), Nanyang Technological University, Division of Physics and Applied Physics, SPMS-04-01, 21 Nanyang Link, Singapore 637371

Yee Chong Loke and Sean J. O'Shea
Institute of Materials Research and Engineering, 3 Research Link, Singapore 117602

Evert Klaseboer
Institute of High Performance Computing, 1 Fusionopolis Way, #16-16 Connexis, Singapore 138632

Boo Cheong Khoo*
Department of Mechanical Engineering, National University of Singapore, Kent Ridge, Singapore 119260 and Singapore-MIT Alliance, 4 Engineering Drive 3, Singapore 117576

Claus-Dieter Ohl
School of Physical and Mathematical Sciences (SPMS), Nanyang Technological University, Division of Physics and Applied Physics, SPMS-04-01, 21 Nanyang Link, Singapore 637371

(Received 4 October 2011; revised manuscript received 28 December 2011; published 17 January 2012)

A method to create impacting jets at the micrometer length scale by means of a collapsing cavitation bubble is presented. A focused shock wave from a lithotripter leads to the nucleation of a cavitation bubble below a hole of 25 μm diameter etched in a silicon plate. The plate is placed at an air-water interface. The expansion and collapse of the bubble leads to two separate jets—an initial slow jet of velocity $\sim$10 m/s and a later faster jet of velocity $\sim$50 m/s. The jets subsequently impact coaxially, resulting in a circular sheet of liquid in the plane perpendicular to their axis. The sheet is characterized by a ring of droplets at its rim and breaks up into a spray as the shock pressure is increased. The results demonstrate an approach to create a high-speed jet and fine spray on demand at the micrometer scale.

DOI: 10.1103/PhysRevE.85.015303 PACS number(s): 47.60.Kz, 47.40.Nm, 47.55.dp

I. INTRODUCTION

Droplets and jets of diameter of the order of micrometers are used in many applications such as in inkjet printing [1], in the manufacture of polymer nanofibers by the electrospinning process [2], encapsulation of the droplets of one liquid within another [3], and liquid jet based needle-free injectors [4]. These applications cover both relatively low speed jets [2,3] as well as high-speed jets [4] and therefore different approaches have been used to create the jets and droplets. In inkjet printing for example, a forced breakup is induced in a continuous jet of ink by the Rayleigh-Plateau instability. Alternatively, an expanding thermal bubble is created within the chamber containing ink, which forces out an ink droplet through an orifice in the chamber. For electrospinning and encapsulation processes [2,3], a thin jet is created from a droplet by applying an electric potential difference between the droplet and a collector plate to form a Taylor cone and jet [5]. For liquid jet based needle-free injectors [4] a pressure difference is created across the ends of a syringe, which leads to a high-speed jet.

In this Rapid Communication, we report on a method to create two impacting jets driven by the expansion and collapse of a cavitation bubble. Previous works, for example Ohl and Ikink [6], have reported on jetting induced in a bubble collapse where an asymmetry due to a pressure gradient or the presence of a boundary leads to fluid focusing in the form of a jet. Here, this jetting flow induced in a bubble near a boundary is used to focus two jets through the hole in a plate situated at an air-water interface. The bubble itself is formed due to the interaction between a shock wave and the holed plate. Earlier studies on impacting jets [7–9] have reported on two jets impinging head-on resulting in a thin sheet of liquid of elliptical shape bordered by a rim of droplets in the plane bisecting the angle between the jets. In the present experiments, a symmetrical sheet of liquid characterized by a ring of droplets is observed resulting from two impacting jets moving in the same direction through a single hole. A slow jet emerges first followed by a faster second jet that catches up with the first jet and impacts with the first one.

II. EXPERIMENTAL SETUP AND PROCEDURE

The experimental setup used in this study is shown in Fig. 1(a). It consists of a modified commercial shock-wave

*mpekbc@nus.edu.sg

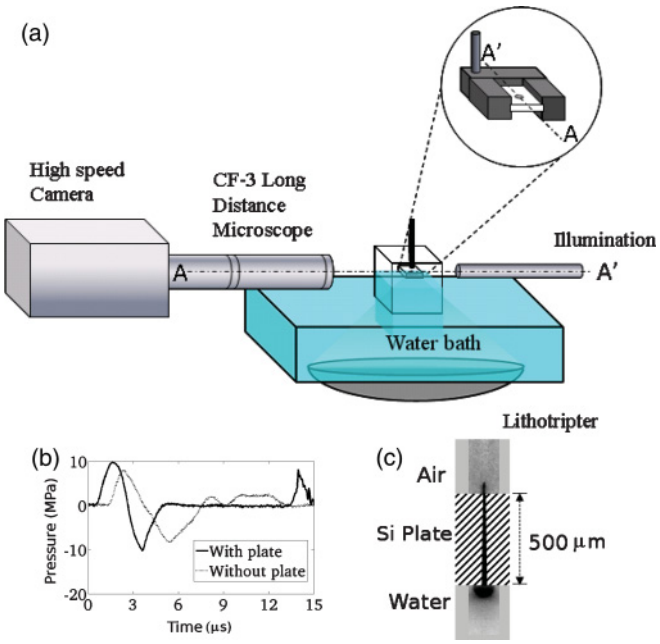

FIG. 1. (Color online) (a) Schematic of the experimental setup used for the study of microjets. Inset: a magnified view of the plate with the hole and its holder. The plate is positioned at the water-air interface. (b) A typical pressure profile measured at the focal point of the shock-wave lithotripter at a voltage setting of 3.50 kV in a free field (dotted black line) and in the presence of a glass plate of size 10×10 mm, thickness 1 mm, and a hole diameter of 800 μm (solid black line). The glass plate was used as a substitute for the silicon plate (0.5 mm thickness, 25 μm hole diameter) so that the needle hydrophone could be placed within the hole for measurement. In the presence of the plate, there is an increase in the peak positive and negative pressures measured and a shortening of the cycle time of the sinusoidal profile as compared to the free-field case. (c) A cross-section view through the hole in the plate indicating the positions where the camera images were recorded (shown by sample images above and below the plate). The plate thickness is to scale.

lithotripter similar to that used in an earlier study [10], a water bath with the transducer of the shock-wave lithotripter fixed at the base, a silicon plate with a hole 20–25 μm in diameter at its center, a custom-built holder to fix the plate in position on the water surface, a high-speed camera (Photron Fastcam SA 1.1 color) and illumination system (Olympus ILP-2 light source) for recording the images, two three-axis translation stages, one each for positioning the plate holder and the camera, respectively, and a digital delay generator.

The plates used in the experiment were made from a silicon wafer (100 orientation, *P*-type wafer with total thickness variation <10 μm) which is polished on the side exposed to the water. The square plates (10×10 mm) have a thickness of 0.50 mm. A hole of diameter ~ 25 μm was etched in the center of the plate using a laser [high power diode-pumped, repetitively *Q*-switched Nd:YAG laser system, 5200 (ESI)]. Because of the laser-etch technique, the hole is slightly tapered with a diameter of ~ 25 μm on the surface where the laser etch was started (polished surface) and a diameter of ~ 20 μm at the other surface.

The plate was positioned on the air-water interface such that the hole is exactly at the focal point of the shock-wave lithotripter. Figure 1(b) shows a typical pressure profile recorded at the focal point of the shock-wave lithotripter using a needle hydrophone (SN 1486, Precision Acoustics Ltd., with a sensor diameter of 0.2 mm) at a voltage setting of 3.50 kV in (a) a free field in water (dotted black line) and (b) within the hole in a plate located at the air-water interface (solid black line). A glass plate (1 mm thickness, 800 μm hole diameter) was used as a substitute for the silicon plate used in experiments (0.5 mm thickness, 25 μm hole diameter) so that the needle hydrophone probe could be placed inside the hole for measurement, i.e., we assume pressure measurements within the 800 μm hole provide a reasonable approximation to the pressures expected within the 25 μm hole. The plate was located at the surface of the water and the probe tip placed within the hole (slightly submerged) during the measurement while for the measurements without the plate (free field), the water was filled to a height of 30 mm above the probe tip. The free-field pressure profile shows a positive peak of 8 MPa at ~ 2.5 μs and a negative peak of -8 MPa at ~ 5.5 μs. The time $t = 0$ μs corresponds to the time when the sinusoidal portion of the pressure waveform first begins. With respect to the triggering of the shock-wave lithotripter, $t = 0$ μs corresponds to a delay of 128 μs from the triggering time. In the presence of the plate the peak pressure values are higher with a positive peak of 10 MPa at ~ 2 μs and a negative peak of -10 MPa at ~ 4 μs. In the presence of the plate, the cycle time for the sinusoidal portion of the profile is shortened to ~ 5 μs as compared to ~ 7 μs for the free-field case.

The interaction of the shock wave with the hole led to cavitation activity below the plate and a jet of liquid emerging from the hole into the air. Both of these regions as shown in Fig. 1(c) were recorded in separate experiments using the high-speed camera and the repeatability of the bubble (i.e., below plate), and the jet (i.e., above plate) formation allowed us to correlate the two recordings in terms of the timing. The setup was illuminated by diffused backlighting and operated at a frame rate of 500 000 frames/s. The trigger delay of the camera with respect to the shock-wave transducer was controlled using a digital delay generator (Model 575 Digital Delay/Pulse generator, BNC Corporation).

III. RESULTS AND DISCUSSION

Figure 2 shows three image sequences of the jet above the plate and the corresponding cavitation bubble observed below the plate for three different pressure settings (distinguished by the different voltage settings 3.25, 4.00, and 4.50 kV). A higher voltage setting results in a shock wave with a larger pressure amplitude. The position of the plate in the images is indicated by the white line in the first frame.

The phenomenon observed on the top of the plate is entirely driven by the bubble which develops below the plate, beginning with the nucleation of the bubble and the subsequent expansion and collapse. Figure 2 shows that the appearance of the bubble at the bottom and the jet on top occurred simultaneously at ~ 8 μs where $t = 0$ μs corresponds to $t = 0$ μs as described in the pressure profile plot. The bubble is formed exactly at the location of the hole. The shock wave is reflected at the air-water

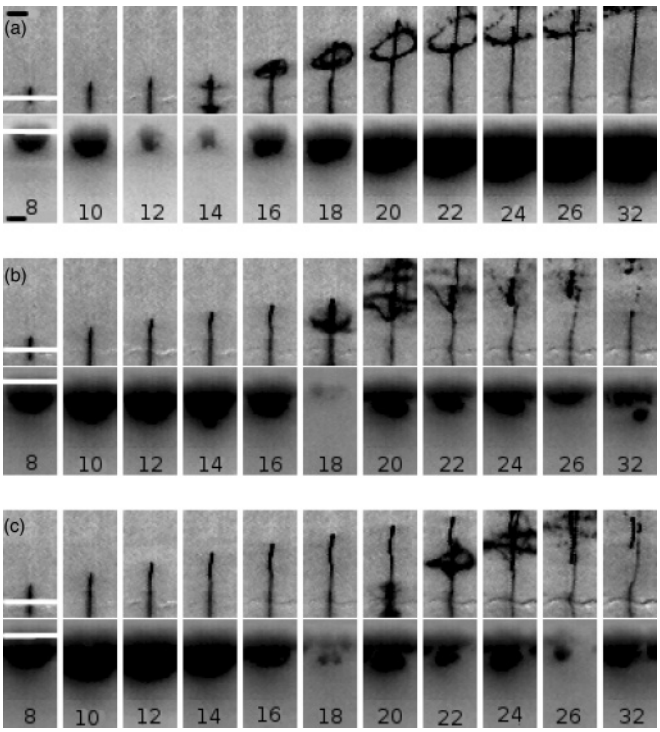

FIG. 2. The evolution of the jet above the hole and the cavitation bubble formed below the hole for increasing shock pressures is shown at (a) 3.25 kV, (b) 4.00 kV, and (c) 4.50 kV. Each sequence is a combination of two separate recordings at the top and bottom of the plate. There is a correlation between the first collapse of the bubble and the appearance of a ring shortly afterward. Note the change in the character of the ring from circular to irregular shape, the increase in the cavitation bubble size, and the consequent delay in the collapse of the bubble and ring formation as the shock strength is increased. The scale bar shown corresponds to a length of 100 μm. The position of the plate is indicated with a solid white line in the first image of each sequence (top and bottom). The numbers at the bottom of each image sequence indicate the time in microseconds.

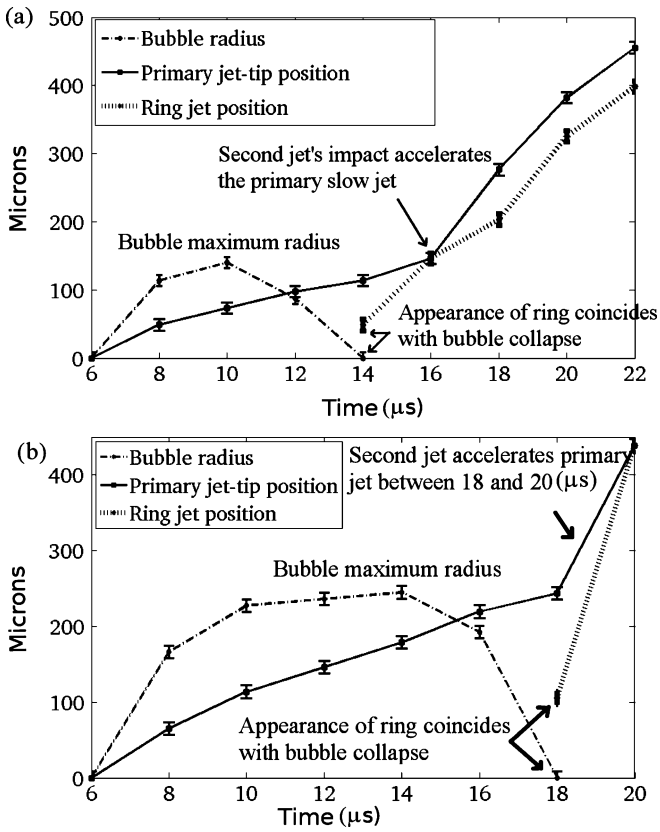

FIG. 3. The variation of the jet-tip position, bubble radius, and ring position with time for the voltage settings of (a) 3.25 kV and (b) 4.00 kV are shown corresponding to the cases shown in Figs. 2(a) and 2(b). The jet-tip and ring positions are measured with reference to the surface (air side) of the plate. The primary jet-tip positions show an increase in their slope after the secondary jet impacts the primary jet indicating the acceleration of the jet due to the impact. The error bars correspond to the error in the measurement of position.

interface through the hole and consequently a tensile pressure is created inside the hole which leads to bubble nucleation. The times of the bubble's appearance and the negative peak in the pressure profile measurements supports the possibility that the negative peak pressure led to the bubble nucleation. The pressure profile [Fig. 1(b)] shows that in the presence of a plate, the negative pressure peak is reached at $t = 4$ μs ($t = 6$ μs for the free-field case). The bubble is first observed at a visible size at $t = 8$ μs, which corresponds to 1 to 2 frames after the negative peak pressure (based on the frame rate used). As the bubble expands while attached to the hole, it pushes some of the fluid within the hole into the form of a jet which is expelled from the other side. This jet is henceforth called the "primary slow jet."

The bubble expanded to a maximum radius which increased with an increase in the voltage used (from 140 μm for 3.25 kV to 270 μm for 4.50 kV) and then collapsed. A second cavitation zone is also observed below the plate for all the pressure settings after the collapse of the bubble. This cavitation zone, however, does not have a visible effect on the evolution of the jet. The second cavitation zone could have formed due to a lowering of the pressure in the region from reflected shock waves.

Around 0–2 μs after the bubble collapsed, a liquid ring emerged above the plate for all the voltage settings. The ring formation was delayed with an increase in the shock pressure. This corresponds to a delay in the bubble collapse resulting from an increase in the bubble diameter and suggests that the ring structure is probably a consequence of the bubble collapse. An oscillating bubble close to a rigid boundary is known to collapse with a jet directed toward the boundary [11–18]. A question that then arises is—does the observed ring result from this second jet due to the bubble collapse?

To explore this possibility, the position of the jet tip, the variation of the bubble radius, and the position of the ring jet are plotted as a function of time for two different pressure settings (3.25 and 4.00 kV) in Fig. 3. Consider Fig. 3(a) for the 3.25 kV setting. The first appearance of the ring coincides with the bubble collapse. For the jet-tip position, there are two different slopes observed. Initially, the jet-tip position moves linearly with time until $t = 14$ μs. After the ring jet collides with the primary slow jet (i.e., after $t = 14$ μs), the variation of the jet-tip position shows an increased slope indicating an

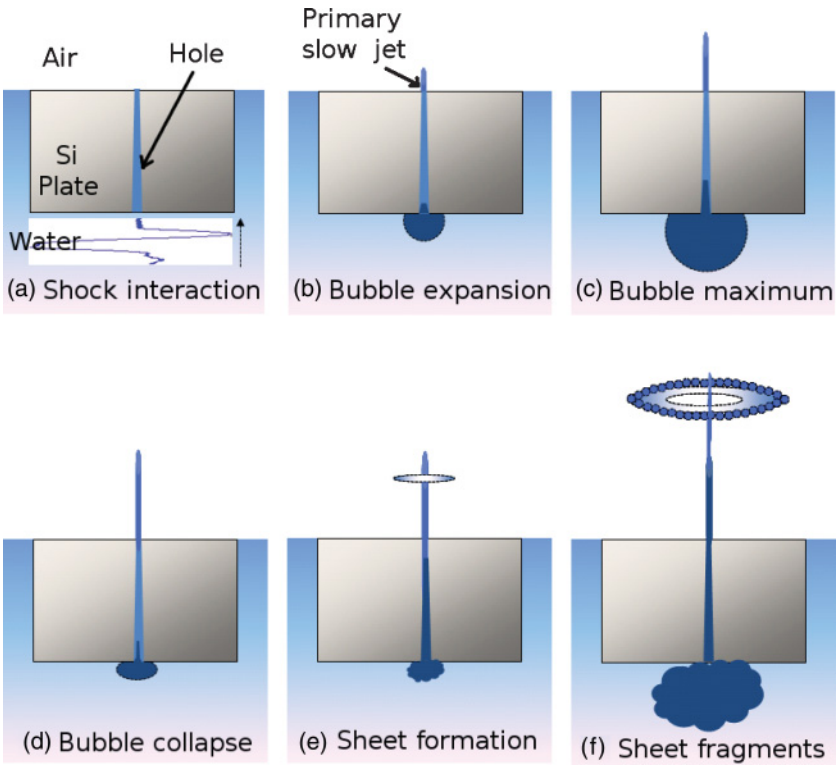

FIG. 4. (Color online) The mechanism behind the formation of the ring and jet structure is illustrated. (a) The focused shock wave interacts with the holed plate, leading to nucleation of a cavitation bubble at the location of the hole. (b) The cavitation bubble expands at the bottom of the hole leading to part of the liquid present in the hole to emerge as a primary slow jet. (c) The bubble reaches its maximum size and the jet simultaneously moves forward. (d) The bubble collapses with a jet directed toward the boundary (plate) leading to a second faster jet through the hole. (e) The faster jet impacts coaxially with the primary slow jet and leads to a thin sheet of liquid expanding radially from the jet axis and perpendicular to it. The sheet has a rim of droplets, i.e., the ring. (f) The jet is accelerated due to the impact and the sheet also begins to fragment as observed from the increasing diameter of the ring of droplets (and a spray at higher pressure). A second cavitation zone is also observed below the plate, possibly due to reflected shock waves.

acceleration of the jet tip. A similar observation is seen for Fig. 3(b), which corresponds to 4.00 kV.

The observations suggest that upon bubble collapse, a faster second jet impacts with the primary slow jet, leads to a ring, and also imparts an acceleration to the jet tip. The jet-tip velocities were calculated and show an increase from ~10 m/s before to ~50 m/s after the ring reached the jet tip. As noted earlier, the ring itself was observed only after the bubble collapsed and its formation was delayed when there was a delay in the bubble collapse. Therefore it is deemed likely that the bubble collapsed, producing a second faster jet which accelerated the primary slow jet and also led to the observed ring. Impinging jets in head-on impact have been reported to form a thin sheet of liquid of elliptical shape [7–9] bordered by a thicker rim of liquid droplets. It appears that an impact between the second jet and the primary slow jet results in a similar liquid sheet which is circular in shape (due to the coaxial impact) and has a thick rim of droplets. The present case differs from the earlier studies in that both the impinging jets are moving in the same direction and differ in their velocity.

The sequences Figs. 2(a)–2(c) also show that as the shock pressure increases the ring tends to lose its circular character and breaks up into a spray. The larger bubble formed at a higher shock pressure results in a stronger impact between the two jets upon bubble collapse and consequently, a more unstable liquid sheet.

The likely sequence of events leading to the formation of the jet with the surrounding ringlike structure is summarized in Fig. 4 and described as follows: When a plate with a hole of a few micrometers diameter is immersed in water, and subject to a focused shock wave, the interaction of the shock wave with the holed plate leads to nucleation of a cavitation bubble below the hole [Fig. 4(a)]. As the bubble expands while attached to the hole, it pushes and expels part of the liquid within the hole to form a primary slow jet [Figs. 4(b) and 4(c)]. The bubble subsequently collapses toward the plate and a second faster jet is formed which moves through the hole [Fig. 4(d)]. The fast moving second jet collides with the primary jet [Fig. 4(e)]. In this collision a thin sheet spreading radially from the jet axis is formed. Later the sheet fragments. After fragmentation, only the ring of droplets bordering the rim can be distinguished [Fig. 4(f)]. If the shock pressure is increased, a stronger jet impact results leading to an unstable liquid sheet and fragmentation into a spray rather than the stable ring observed at lower shock pressure.

IV. CONCLUSIONS

In this Rapid Communication, the mechanism of jet impact between two jets formed through a hole of a few micrometers diameter in a plate at an air-water interface has been studied using a high-speed camera. The entire phenomenon is driven by the formation, expansion, and subsequent collapse of a cavitation bubble created at the location of the hole. The bubble expansion leads to a primary slow jet and the subsequent collapse to a faster second jet, both moving through the hole. The interaction between the two jets moving at different velocities leads to a thin sheet of liquid with a ring of droplets forming its rim in a plane perpendicular to the jets. The second jet collides with the primary slow jet, leads to the formation of a radially expanding liquid sheet from the jet axis, and an increase in the velocity of the primary jet. The sheet later fragments into a spray. The results suggest a method that could be used to create a high-speed jet of fluid with potential application to biomedicine, such as transdermal drug delivery through liquid jet injectors, or atomization of liquid jets into sprays.

[1] B.-J. de Gans, P. Duineveld, and U. Schubert, Adv. Mater. **16**, 203 (2004).
[2] D. H. Reneker and A. L. Yarin, Polymer **49**, 2387 (2008).
[3] I. G. Loscertales, A. Barrero, I. Guerrero, R. Cortijo, M. Marquez, and A. M. Gañán-Calvo, Science **295**, 1695 (2002).
[4] S. Mitragotri, Nat. Rev. Drug Discovery **5**, 543 (2006).
[5] G. Taylor, Proc. R. Soc. London, Ser. A **280**, 383 (1964).
[6] C. D. Ohl and R. Ikink, Phys. Rev. Lett. **90**, 214502 (2003).
[7] M. F. Heidmann, R. J. Priem, and J. C. Humphrey, A study of the sprays formed by two impinging jets, NACA-TN-3835, 1957 (unpublished).
[8] N. Dombrowski and P. C. Hooper, J. Fluid Mech. **18**, 392 (1964).
[9] N. Bremond and E. Villermaux, J. Fluid Mech. **549**, 273 (2006).
[10] B. M. Borkent, M. Arora, C.-D. Ohl, N. de Jong, M. Versluis, D. Lohse, K. A. Mørch, E. Klaseboer, and B. C. Khoo, J. Fluid Mech. **610**, 157 (2008).
[11] M. Kornfeld and L. Suvorov, J. Appl. Phys. **15**, 495 (1944).
[12] A. Vogel, W. Lauterborn, and R. Timm, J. Fluid Mech. **206**, 299 (1989).
[13] A. Philipp and W. Lauterborn, J. Fluid Mech. **361**, 75 (1998).
[14] Y. Tomita and A. Shima, J. Fluid Mech. **169**, 535 (1986).
[15] B. Karri, K. S. Pillai, E. Klaseboer, S.-W. Ohl, and B. C. Khoo, Sens. Actuators A **169**, 151 (2011).
[16] B. C. Khoo, E. Klaseboer, and K. C. Hung, Sens. Actuators A **118**, 152 (2005).
[17] K. S. F. Lew, E. Klaseboer, and B. C. Khoo, Sens. Actuators A **133**, 161 (2007).
[18] E. Klaseboer and B. C. Khoo, Comput. Mech. **33**, 129 (2004).